GA–A25799

BENCHMARKING OF ALTERNATE THEORIES FOR STARK BROADENING AGAINST EXPERIMENTAL DATA FROM DIII-D DIAGNOSTICS

by
N.H. BROOKS, S. LISGO, E. OKS, D. VOLODKO,
M. GROTH, A.W. LEONARD, and the DIII-D TEAM

MAY 2007

GENERAL ATOMICS

DISCLAIMER

GA–A25799

BENCHMARKING OF ALTERNATE THEORIES FOR STARK BROADENING AGAINST EXPERIMENTAL DATA FROM DIII-D DIAGNOSTICS

by
N.H. BROOKS, S. LISGO,*,† E. OKS,‡ D. VOLODKO,‡
M. GROTH,§ A.W. LEONARD, and the DIII-D TEAM

This is a preprint of a paper to be presented at the XII All Russia Conference on High Temperature Plasma Diagnostics, June 3–8, 2007 in Zvenigorod, Russia and to be published in the Proceedings.

*University of Toronto Institute for Aerospace Studies, Toronto, Canada
†UKAEA Fusion Association, Culham Science Centre, Abingdon, UK
‡Physics Department, Auburn University, Auburn, Alabama, USA
§Lawrence Livermore National Laboratory, Livermore, California, USA

Work supported by
the U.S. Department of Energy
DE-FC02-04ER54698, W-7405-ENG-48

GENERAL ATOMICS PROJECT 30200
MAY 2007

GENERAL ATOMICS

ABSTRACT

Spectroscopy of high-n, Balmer line transitions provides a means of measuring n_e and T_e in recombining plasmas [J.L. Terry *et al.*, Phys. Plasmas **5** (5), 1579 (1998).] The relative intensities of Rydberg series lines near the ionization limit are a sensitive diagnostic of T_e, for $T_e < 1.5$ eV. Stark broadening of these same lines provides a measure of local n_e and, with less accuracy, of T_e. The accuracy of different theoretical models for Stark broadening [H.R. Griem, *Spectral Line Broadening by Plasmas*, New York, 1974; E. Oks, *Stark Broadening of Hydrogen and Hydrogenlike Spectral Lines in Plasmas: The Physical Insight*, Alpha Science International, Oxford, UK, 2006] is evaluated by comparing values of n_e and T_e measured on DIII-D by divertor Thomson scattering (DTS) with those deduced from spectral profile analysis of Balmer series deuterium lines. In particular, the detailed dependence of line width on principal quantum number provides a sensitive metric for distinguishing which model best accords with experiment.

I. INTRODUCTION

The high heat load to first wall components in next generation devices [1] presents a serious lifetime issue for any material surface. The physics solution envisaged for ITER relies on a thick neutral gas target to dissipate the energy and momentum carried by the plasma streaming along open field lines to poloidal divertor plates. This so-called detached divertor condition is characterized by a reduced ion flux reaching the target plates, and a high electron density and low temperature in the divertor volume where plasma intermixes with neutral gas [2]. In this plasma "flame out" region, three-body recombination generally provides the dominant mechanism for the population of high-n levels whose radiative decay gives rise to the deuterium Balmer (n_{lower} = 2) and Paschen (n_{lower} = 3) series line emission. Stark broadening of these bright Rydberg series lines provides a valuable diagnostic of the local n_e. However, alternate theories of Stark broadening give different predictions for the n_e, T_e regime typical of detached divertors in existing tokamak devices.

The present study takes advantage of the excellent diagnostic set on the DIII-D tokamak to compare the accuracy of different Stark broadening analysis methods [3,4]. In particular, DIII-D's divertor Thomson scattering (DTS) system is used to provide an independent measurement of n_e. A series of identical repeat discharges, run as part of a surface deposition experiment involving toroidally uniform injection of isotopically tagged methane, gave the opportunity to scan spectrometer wavelength between shots and to accumulate improved photon statistics for Thomson analysis.

Modeling efforts on other devices with detached divertor operation have been hampered by experimental uncertainties in the measurement of n_e. In particular, on the Alcator C-Mod tokamak, where very extensive spectroscopic studies of detachment were carried out [5–7], comparison of the spectroscopic and Langmuir probe data sets with output from the "OSM-EIRENE" plasma reconstruction code gave agreement which was only marginally within experimental uncertainties [8]. In this case, n_e was deduced from the Stark broadening of high-n Balmer lines using conventional theory [4]. Because of the highly nonlinear dependence of volume recombination processes on both n_e and T_e when T_e is less than 1 eV [9], accurate experimental measurements are critical to an improved simulation of the detached divertor condition; this need for reliable measurements of n_e motivates the present effort to benchmark different Stark broadening theories.

II. EXPERIMENTAL SETUP

DIII-D is a medium size, diverted tokamak with major radius R = 1.66 m and minor radius a = 0.67 m [10]. The discharge investigated has a lower single null in the poloidal magnetic field, line averaged electron density $\bar{n}_e = 8.1\times10^{19}$ m^{-3} during the flat-top, axial toroidal field of B_T = 2 T, plasma current of I_p = 1.1 MA, and 6.6 MW of neutral beam heating, with the $B\times\nabla B$ drift toward the lower divertor. Time traces of the principal plasma parameters are shown in Fig. 1. Enhanced confinement, or H-mode, is indicated by the rapid fluctuations in divertor D_α light caused by edge localized modes, or ELMs [11]. These MHD instabilities are associated with the periodic expulsion from the confined plasma region of energetic particles, which then stream along open field lines to the walls of the vacuum vessel. The average time between ELMs, τ_{ELM}, for this discharge is ~5 ms.

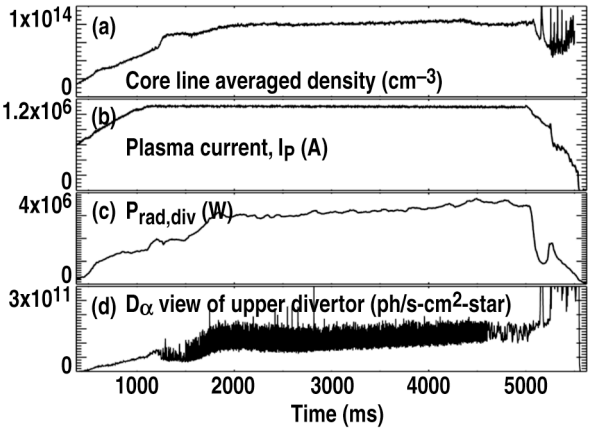

Fig. 1. Relevant time traces for discharge 123410. (a) Average plasma density in the confined plasma (core), (b) plasma current, (c) radiated power in the divertor region, (d) fast D_α trace (20 kHz sampling) in the upper divertor (a lower divertor view was not available). The high-frequency D_α fluctuations indicate rapid ELMs.

The line shapes of the high-n Balmer series lines ($n \rightarrow 2$, with n ranging from 6 to 10) are measured in the wavelength interval 380 < λ < 410 nm along four vertical paths through the divertor that are closely space in major radius about R = 1.49 m. A schematic cross section of the lower divertor is presented in Fig. 2, along with the diagnostic lines-of-sight of interest here. The Czerny-Turner spectrometer has an instrumental broadening of ~ 0.2 nm and a dispersion of 0.0226 nm/pixel. The divertor plasma density in these discharges is high enough and the temperature low enough, that the high-n Balmer lines exhibit Stark broadening significantly greater than the instrumental broadening which, in turn, exceeds that due to magnetic Zeeman splitting by more than a factor of 5. The calculated full width at half maximum (FWHM) of the blended π and σ magnetic components is less than 0.04 nm for the field at R = 1.49 m in the

DIII-D divertor. Unfortunately, the spectrometer integration time is 10 ms, or approximately two ELM periods, so the measured FWHMs of these lines are always ELM-averaged quantities, complicating the analysis; see Section 3.

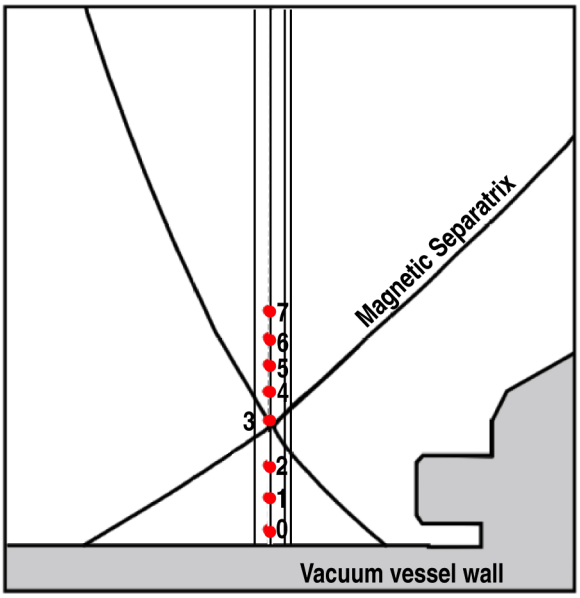

Fig. 2. Poloidal magnetic configuration of the DIII-D lower divertor region, with high-resolution spectrometer views (vertical lines) and divertor Thomson channels (dots, labelled 0 to 7) superposed. The "separatrix" flux surface divides the plasma cross section into an interior region of nested, closed flux surfaces and an exterior region of open flux surfaces; plasma within the separatrix is magnetically confined, that without is free to stream along open field lines to the walls of the containment vessel. The PFR is the triangular space below the X-point, enclosed between the legs of the separatrix and the vessel wall.

The DTS system [12] views the electron-scattered light from a Nd:YAG laser at eight points along its vertical path, measuring n_e and T_e (for $T_e > \sim 1$ eV). Each laser pulse lasts only 10 ns, a duration much shorter than the interval between ELMs, τ_{ELM}; the laser pulse repetition rate is 50 Hz. The laser is at the same radial location as the high-resolution spectrometer's central view, but displaced toroidally, allowing a direct comparison of $n_{e,Stark}$ and $n_{e,DTS}$ at identical points in the poloidal plane.

The tomographic inversion of a tangentially viewing 2D CCD camera image shows the poloidal distribution of D_γ $(5 \rightarrow 2)$ in the divertor [13,14]; see Fig. 3 [15], where the inversion was performed for a 1 ms integration period shortly after the intensity peak in divertor D_α. Assuming D_γ to be representative of the higher-n Balmer lines, the emission along the spectrometer line-of-sight is clearly localized to the private flux region (PFR) below the X-point. As a result, only channels 0–3 of the DTS system need to be considered in the present analysis.

Images of C III from the same 1 ms time period indicate that the divertor is partially detached on both the inner and outer target plates.

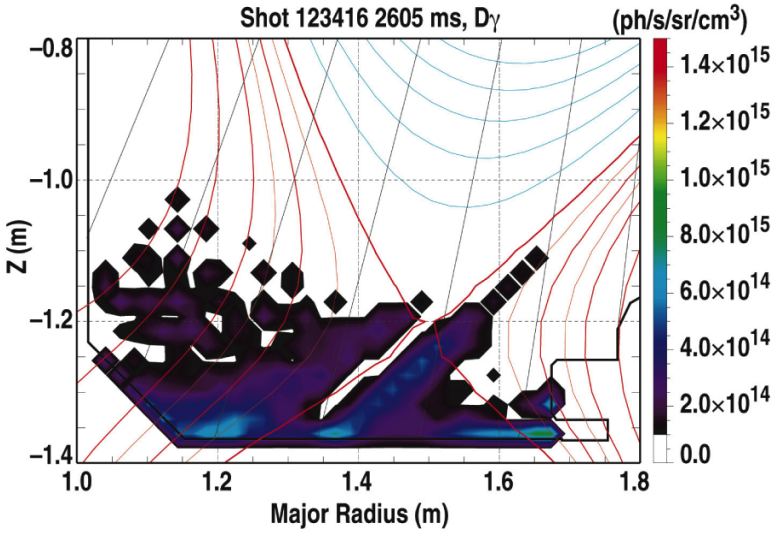

Fig. 3. Tomographic inversion of 2D CCD tangentially viewing camera image of the divertor, in D_γ light. The emission is concentrated in the PFR, so that only this region needs to be considered in the DTS analysis. [Courtesy of M. Groth, *et al.*, Phys. Plasmas **14**, 056120 (2007).]

III. ANALYSIS OF DIVERTOR THOMSON DATA

As stated in the introduction, the objective is to compare estimates of n_e from Stark broadening analysis with n_e data from DTS, in an effort to evaluate the accuracy of competing Stark broadening models. Unfortunately, the divertor plasma fluctuations related to ELMs are substantial, as seen in Fig. 1(d), which means that the measured Stark broadened density is a function of the density variation over the ELM. Therefore, a comparison with $n_{e,DTS}$ requires the calculation of a weighted average ($\tau_{DTS} \ll \tau_{ELM}$) over the ELM, and over the line of sight:

$$\langle n_{e.div} \rangle = \int_{Z_0}^{Z_x} \int_{0}^{t_{ELM}} \varepsilon(Z,t) n_{e,div}\, dt\, dZ \quad , \tag{1}$$

where Z is the vertical coordinate along the line-of-sight, t is time, and ε is the normalized emissivity of the high-n Balmer line that is used as the weight function. The spatial variation of the divertor plasma along the spectrometer view, as indicated by the D_γ inversion in Fig. 3, is (coarsely) resolved by the four DTS channels between the X-point and the divertor floor. The DIII-D discharge being investigated was successfully repeated 22 times, giving excellent samples of the temporal variations of n_e and T_e over the ELM cycle.

The DTS data for channels 0 to 3 were reordered relative to the elapsed time t_{ELM} between each of the periodic laser pulses and the onset of the preceding ELM, using a library of ELM profile analysis tools [16]. These data were subsequently filtered to exclude atypical ELMs, i.e., those where the D_α peaks more than 1 ms after the start of the ELM and the time to the start of the next ELM lies outside the range 4.5–6 ms. Linearly interpolating along Z between polynomial fits to the filtered data sets for each of the four channels 0–3, the $n_e(Z,t)$ and $T_e(Z,t)$ profiles shown in Fig. 4 were obtained for the spectrometer line-of-sight coincident with the laser path. The $\varepsilon[n_e(Z,t), T_e(Z,t)]$ values in Eq. (1) are then set to the emissivity for a given high-n Balmer transition using the ADAS database [17]; see Fig. 4(c). Given the detached divertor plasma conditions in these discharges, it is assumed that the high-n emissions are dominated by volume recombination processes and that $n_{D+} = n_e$ locally.

The above exercise gives $\langle n_{e,div} \rangle = 6.0 \pm 0.5 \times 10^{20}\ \mathrm{m}^{-3}$ when only considering uncertainties related to the interpolation process. If the stated uncertainties in the individual DTS data measurements are also included, then the absolute error increases to $\langle n_{e,div} \rangle = 6.0 \pm 1.1 \times 10^{20}\ \mathrm{m}^{-3}$. The average density depends weakly on the particular high-n line that is used as the weight function.

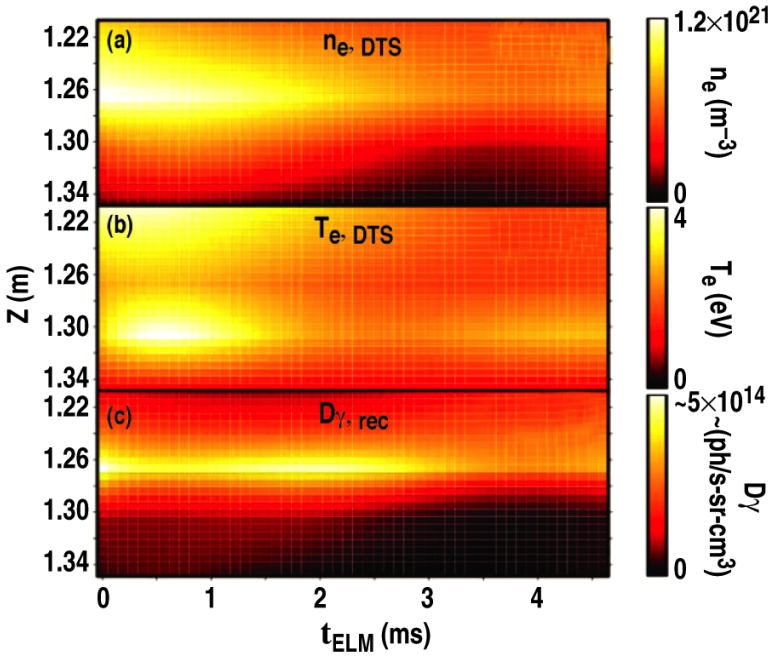

Fig. 4. Divertor Thomson scattering data interpolated temporally over an ELM cycle and spatially between the lower divertor floor and X-point. The Balmer line emissivity provides the weight function for averaging $n_{e,DTS}$ along the spectrometer line-of-sight. The D_γ signal from volume recombination is shown here, and there is little variation in the distribution for the higher-n lines.

IV. MODELING OF STARK BROADENING OF HIGHLY EXCITED BALMER LINES

Figure 5 shows the shapes of the measured high-n deuterium Balmer lines with n_{upper} = 6–10. Acceptable signal-to-noise ratio was obtained by integrating over the period during which the X-point was held stationary and plasma conditions were constant. The instrumental profile, with a FWHM of ~ 0.2 nm, completely masks the triplet structure associated with Zeeman splitting of the Balmer line, the envelope of that blended triplet structure being less than 0.04 nm wide in all cases. The experimental FWHM values from Fig. 5 are plotted versus n in Fig. 6. Also shown are fits from the "conventional" [4] and "highly-advanced" [3,18] Stark broadening theories.

The highly advanced theory (HAT) [3,18] is based primarily on a generalization of the formalism of dressed atomic states (DAS) in plasmas wherein the monochromatic field previously used to describe the interaction of laser or maser radiation with gases is replaced by a broadband field due to plasma electrons and ions. The employment of the generalized DAS by the HAT [3,18] enables an analytic description of the coupling between electron and ion microfields mediated by the radiating atom. This indirect coupling increases nonlinearly with the principal quantum number n and becomes important for high-n lines even at moderate electron densities. A second outcome of the generalized theory is an accurate analytical treatment for the ion-dynamical broadening, which is obtained in a non-binary description of the ion microfield and without using the impact approximation. For the edge plasmas of tokamaks, ion dynamics is important for Balmer lines originating from levels with $n < 8$. For the above reasons, the application of the HAT to the analysis of experimental high-n lines enhances the accuracy of the density determination and, additionally, yields information about temperature, a plasma parameter which the conventional theory is unable to predict.

From Fig. 6, it is seen that the HAT more accurately reproduces the shape of the experimental FWHM dependence than the conventional theory. The shape of the FWHM dependency in the HAT is more complicated than that in the conventional theory because of the competition of two additional effects included in the HAT, but neglected in the conventional theory, namely, indirect coupling and ion-dynamical broadening. Broadening due to indirect coupling increases with n, while that due to ion-dynamical broadening decreases with n.

The theoretical results presented in Fig. 6 were obtained from the best fit to the shapes of the experimental Balmer lines presented in Fig. 5. The best fit for the conventional theory yields $n_{e,Stark} = 4.5 \pm 0.6 \times 10^{20}$ m^{-3}, but no information about the temperature. The most probable values of the densities, deduced from individual line profiles fitted by the conventional theory, vary by over 15%. The best fit for the HAT yields $n_{e,Stark} = 5.0 \pm 0.5 \times 10^{20}$ m^{-3} and the temperature $T = 1.5 \pm 0.5$ eV. The most probable values of the densities, deduced from individual line profiles fitted by the HAT, vary by less than 5%.

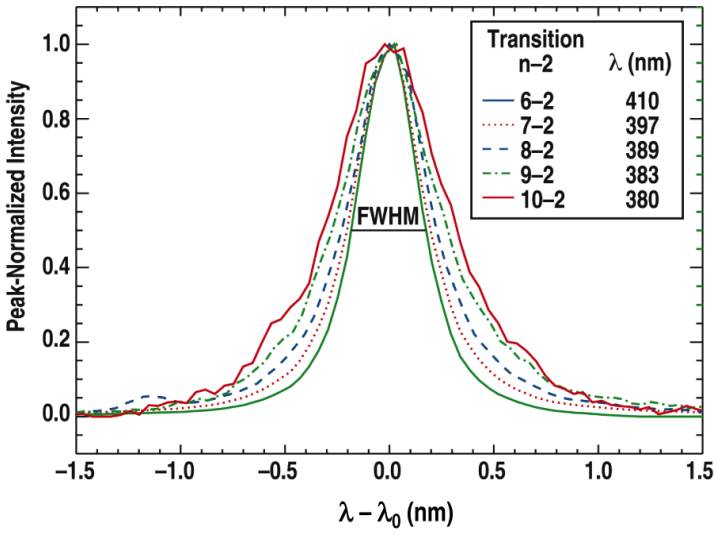

Fig. 5. Profiles of high-n deuterium Balmer lines. The signals were integrated over the portion of the discharge during which conditions were held constant.

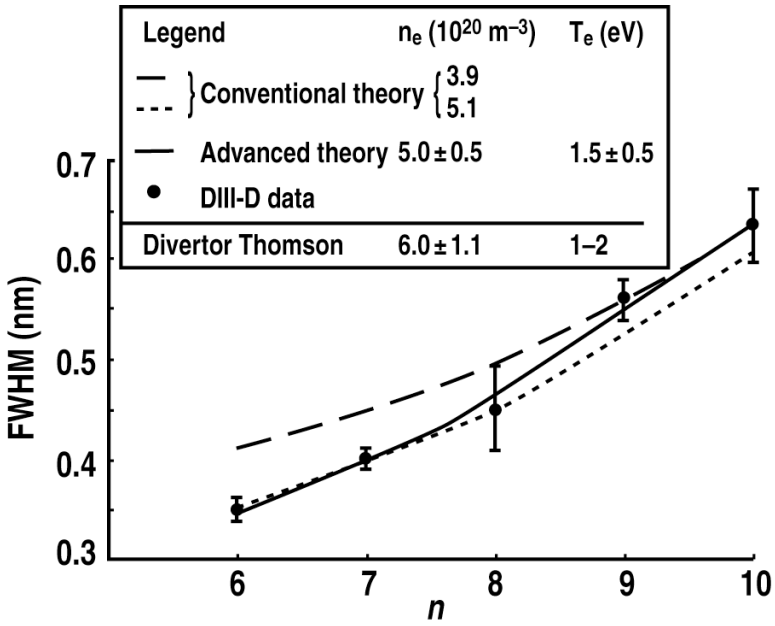

Fig. 6. FWHM (Angstroms) versus the principal quantum number, n, of deuterium high-n Balmer lines, as measured in the DIII-D divertor. Fits for Stark broadening theories are shown: highly advanced theory with $n_e = 5.0 \times 10^{20}$ m^{-3} and $T = 1.5$ eV (solid line), and conventional theory with $n_e = 3.9 \times 10^{20}$ m^{-3} (dashed line) and $n_e = 5.1 \times 10^{20}$ m^{-3} (dotted line).

The plasma parameters deduced from the Stark broadening of the experimental high-n Balmer lines can be now compared with $\langle n_{e,div} \rangle = 6.0 \pm 1.1 \times 10^{20}$ m^{-3} and $T_e = 1$–2 eV

determined from the experimental DTS ELM data. It is seen that the latter agrees with the plasma parameters deduced by the HAT better than with the plasma parameters deduced by the conventional theory. Besides, the analysis employing the HAT allows obtaining both n_e and T, while the conventional theory can determine only n_e and with a much higher error than the n_e deduced via the HAT.

V. DISCUSSION AND CONCLUSIONS

High resolution measurements of Stark broadened high-n Balmer series lines were made for a rapidly ELMing plasma discharge. An ELM-averaged value of n_e was generated from DTS data and compared with that from Stark broadening analysis of the Balmer line FWHMs, but the quality of the DTS analysis was not sufficient to distinguish unequivocally between the conventional and generalized Stark broadening theories. It was clear, however, that the highly advanced theory gave a significantly better match to the distribution of FWHM with n and, therefore, provides a better representation of the experimental data.

REFERENCES

[1] ITER Expert Groups, Nucl. Fusion **39** (12), 2137 (1999).

[2] P.C. Stangeby, Nucl. Fusion **33** (11), 2503 (1993).

[3] B.L. Welch, H.R. Griem, J. Terry, *et al.*, Phys. Plasmas **2** (11), 4246 (1995).

[4] E. Oks, *Stark Broadening of Hydrogen and Hydrogenlike Spectral Lines in Plasmas: The Physical Insight* (Alpha Science International, Oxford, 2006).

[5] J.L. Terry, B. Lipschultz, A.Yu Pigarov, *et al.*, Phys. Plasmas **5** (5), 1579 (1998).

[6] B. Lipschultz, J.L. Terry, C. Boswell, *et al.*, Phys. Plasmas **6** (5), 1907 (1999).

[7] H.R. Griem, *Spectral Line Broadening by Plasmas* (Academic Press, New York, 1974).

[8] S. Lisgo, P.C. Stangeby, J.D. Elder, *et al.*, J. Nucl. Mater. **337-339**, 256 (2005).

[9] S. Lisgo, "Interpretive Modeling of the Alcator C-Mod Divertor," Ph.D. Thesis, University of Toronto, 2003. http://starfire.utias.utoronto.ca/divimp/publications/

[10] J.L. Luxon, T.C. Simonen, R.D. Stambaugh, Fusion Sci. Technol. **48** (2), 807 (2005).

[11] W. Fundamenski, R.A. Pitts, G.F. Matthews, *et al.*, Nucl. Fusion **45** (8), 950 (2005).

[12] S.L. Allen, D.N. Hill, T.N. Carlstrom, *et al.*, J. Nucl. Mater. **241**, 595 (1997).

[13] M. Fenstermacher, W.H. Meyer, R.D. Wood, *et al.*, Rev. Sci. Instrum. **68** (1), 974 (1997).

[14] M. Groth, M.E. Fenstermacher, J.A. Boedo, *et al.*, J. Nucl. Mater. **313**, 1071 (2003).

[15] M. Groth, S.L. Allen, J.A. Boedo *et al.*, Phys. Plasmas **14**, 056120 (2007).

[16] G.D. Porter, T.A. Casper, J.M. Moller, Phys. Plasmas **8** (12), 5140 (2001).

[17] H.P. Summers, N.R. Badnell, M.G. O'Mullane, *et al.*, Plasma Phys. Controlled Fusion **44**, B323 (2002).

[18] E. Oks, *Stark Broadening of Hydrogen and Hydrogenlike Spectral Lines in Plasmas: The Physical Insight* (Alpha Science International, Oxford, 2006).

ACKNOWLEDGMENTS

This research supported by the U.S. Department of Energy under DE-FC02-04ER54698, W-7405-ENG-48, and by a Collaborative Research Opportunities Grant from the Natural Sciences and Engineering Research Council of Canada.